Temperature Distribution in a Gaussian End-Pumped Nonlinear KTP Crystal: the Temperature Dependence of Thermal Conductivity and Radiation Boundary Condition

Mohammad Sabaeian, Fatemeh Sedaghat Jalil-Abadi, Mostafa Mohammad Rezaee, Alireza Motazedian & Mohammadreza Shahzadeh

Brazilian Journal of Physics

ISSN 0103-9733

Braz J Phys
DOI 10.1007/s13538-014-0291-x

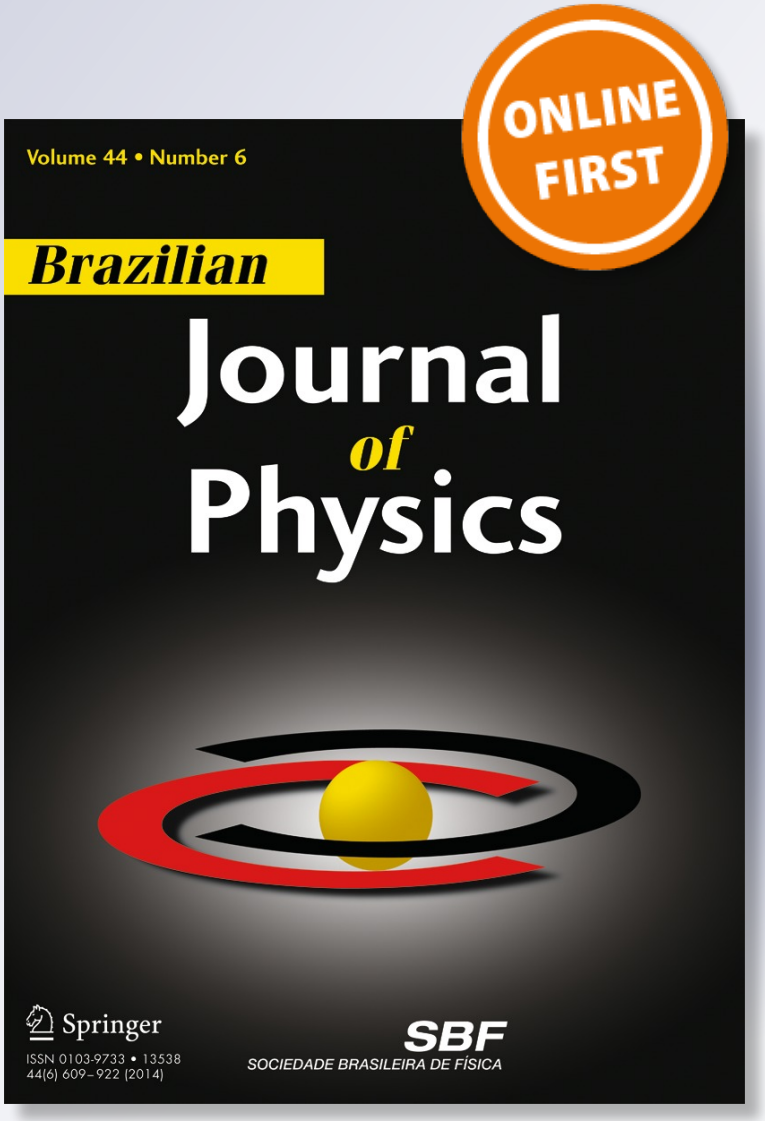

Springer

Braz J Phys
DOI 10.1007/s13538-014-0291-x

ATOMIC PHYSICS

Temperature Distribution in a Gaussian End-Pumped Nonlinear KTP Crystal: the Temperature Dependence of Thermal Conductivity and Radiation Boundary Condition

Mohammad Sabaeian · Fatemeh Sedaghat Jalil-Abadi · Mostafa Mohammad Rezaee · Alireza Motazedian · Mohammadreza Shahzadeh

Received: 23 July 2014 /

Abstract The presence of a temperature-dependent thermal conductivity and the heat radiation boundary condition in the diffusion-type heat equation driven by a Gaussian source make it impossible to find an analytical solution for temperature distribution in the solid-state laser media. In this work, a temperature distribution for a solid-state end-pumped KTP ($KTiOPO_4$) crystal under a Gaussian continuous wave as a heat source is reported. More precisely, the effects of considering the temperature-dependent nature of the thermal conductivity of the KTP crystal and the heat radiation from the end faces of the crystal, in addition to heat convection, which are usually ignored, were studied. It was shown that considering the temperature dependence of thermal conductivity leads to significantly different results compared to constant thermal conductivity case. In addition, it was shown that the radiation can be influential for crystals with large surfaces from which the radiation can occur. Making the crystal thinner, the radiation impact becomes negligible and can be ignored.

Keywords Heat equation · Nonlinear KTP crystal · End-pumping · Temperature · Radiation · Convection

1 Introduction

Green light lasers have found applications in fields of material processing, biology, ophthalmology, printing, spectroscopy, under-water communications, display technology, medicine, industry, and pumping of solid-state lasers [1]. Continuous waves (CW) green light lasers are being used as pumping sources of Ti:sapphire lasers [2] and generating optical parametric oscillators [3].

Nonlinear processes are among the favorite methods to generate green light [4]. Crystals such as KTP [5], LBO [6], BBO [7], and Mg:PPLN [8] are famous for their superior properties. Among them, KTP features unique thermal and optical properties [9]. KTP possesses high nonlinear convection coefficient (d_{eff}=7.3 pm/V), high acceptance angles, high threshold damage, high thermal conductivity [9], and small walk-off angle [10]. The transmission range of KTP ranges from 350 to 4400 nm covering ultraviolet to mid-infrared range of the spectrum [11]. The matching range of KTP crystal ranges from 990 to 3300 nm [11]. With respect to these points, KTP is an excellent choice to be used as a green-light source pumped with output of solid-state lasers such as Nd:YAG and Nd:YVO_4 [12].

Generation of heat in nonlinear crystals during the pumping and second harmonic generation process as a result of optical absorption [13] leads to increase in the crystal temperature [14]. The generated heat in the crystal, hence, causes undesirable effects such as thermal lensing and phase mismatching [15], thermal birefringence [16], reduction in output efficiency [17], and beam quality degradation [14]. These detrimental effects dominate much more in high-power systems [18]. Therefore, calculation of temperature distribution in the crystal is of importance. The amount of heat loaded in the crystal determines the cooling systems needed [16]. If the crystal size is not appropriately selected (relative to pump power), the thermal effects may destroy it [19]. Furthermore, effective cooling systems play a pronounced role in decreasing the detrimental thermal effects [20].

Several researchers have investigated the thermal problem of the laser systems numerically and/or analytically. However, they usually took advantage of simple models such as

M. Sabaeian (✉) · F. S. Jalil-Abadi · M. M. Rezaee · A. Motazedian · M. Shahzadeh
Physics Department, Faculty of Science, Shahid Chamran University of Ahvaz, Ahvaz 61357-43135, Iran
e-mail: sabaeian@scu.ac.ir

Published online: 19 December 2014

considering constant physical parameters and Dirichlet boundary condition for temperature [14]. One of these physical variables, which most often is considered as a constant, is thermal conductivity. Thermal conductivity plays a crucial role in cooling the laser medium. It is of importance for nonlinear materials having higher thermal conductivity to better exchange heat with the environment [21].

Here is worth mentioning some previous investigations regarding thermal modeling of the laser crystals. Pfistner et al. [22] solved the steady-state heat equation for end-pumped Nd:YAG, Nd:GSGG, and Nd:YLF rods using finite element method. The phase mismatching in KTP and LBO crystals due to the heat load was calculated by Seidal and Mann [23]. Weber et al. [24] solved the steady-state heat equation for Nd:YAG rods numerically. They ignored z-derivatives of the heat equation and only considered the radial variations [24]. They took also the advantage of the heat-convection boundary condition [24]. The steady-state heat equation for the laser rods along the radius and using heat-convection boundary condition was solved by Schmid et al. [16]. Thermal conductivity of a self-frequency-doubling Nd:LYAB crystal was investigated by solving the steady-state heat equation [25]. Borise et al. solved the steady-state heat equation in the cylindrical coordinates by considering a constant thermal conductivity and heat-convection boundary condition, analytically [26]. In order to calculate the thermal lensing in Nd:YVO_4 crystal, the steady-state heat equation was solved by considering the thermal conductivity tensor and heat-convection boundary condition [27]. The steady-state heat equation was solved, in a two-dimensional Cartesian coordinate system, for a KTP crystal under a Gaussian CW source [10]. In the work of [10], the authors did not consider the variations of pump power along the crystal as well as the temperature dependence of thermal conductivity [10]. The same conditions were used to investigate the thermal effects in high-power green lasers using KTP crystal [28]. In order to study the thermal effects in Nd:YVO_4/YVO_4 lasers, Li et al. solved the steady-state heat equation in 3D Cartesian coordinates. They considered thermal conductivity as a constant parameter [29]. A semi-analytical solution to the steady-state heat equation was presented by Shi et al. for a Nd:YAG crystal with constant temperature boundary condition [30]. More recently, Sabaeian et al. [31] solved the anisotropic steady-state heat equation by considering the Robin boundary condition for six sides of a cubic crystal in Cartesian coordinate analytically. In addition, the steady-state heat equation was solved for an orthotropic lasing medium under a Gaussian- and a top-hat-laser source by considering the heat-convection boundary condition [14].

In order to investigate the effects of heat on the laser rate equations, Sayahian et al. [32] solved the steady-state heat equation using a constant thermal conductivity and heat convection boundary condition. For fiber systems, Sabaeian [33] showed that the heat radiating from a fiber laser surface is so influential in determining the fiber temperature such that to get a factual answer, it should be taken into account in modeling. However, he showed that considering the temperature dependence of thermal conductivity cannot be such effective. The former results from the large surface/volume ratio, and the latter results from the minor changes of thermal conductivity of silica glass by temperature. Furthermore, in order to study the thermally induced birefringence in solid-core photonic crystal fiber lasers, the same conditions were considered by Mousavi et al. [34] in solving the heat equation. Most recently, Sabaeian and Nadgaran solved the long transient heat equation analytically by considering a constant thermal conductivity and ignored the absorption of the Gaussian source within a finite radius liquid sample in dual-beam mode-mismatched thermal lens spectroscopy [35].

Since the thermal processes are responsible for reduction of the efficiency in nonlinear lasers [23], solving the heat equation with the least approximations and maximum accuracy is necessary. Accordingly, in this work, the long transient heat equation is solved for a nonlinear KTP crystal under an end-pumped Gaussian CW source, with attempt to reduce the approximations already used in the literature. The numerical calculations for the nonlinear (because of temperature dependence of thermal conductivity) and inhomogeneous heat equation with convection and radiation boundary conditions (which is famous as nonlinear boundary condition) were performed by a home-made code based on the finite difference method (FDM) written in Intel Fortran (IFORT).

2 Theory

The time-dependent temperature distribution in solids is obtained by solving the following heat equation [26]:

$$\rho c\frac{\partial T\left(\vec{r},t\right)}{\partial t}-\vec{\nabla}.\left[K(T).\vec{\nabla}T\left(\vec{r},t\right)\right]=Q\left(\vec{r}\right), \tag{1}$$

where $T\left(\vec{r},t\right)$ is the temperature, ρ is the mass density, c is the specific heat, $K(T)$ is the temperature-dependent thermal conductivity, and $Q\left(\vec{r}\right)$ is the heat source. In this work, we considered a Gaussian source given as follows [31]:

$$Q\left(\vec{r}\right)=Q_0\exp\left(-2r^2/\omega_0^2\right)\exp(-\alpha z), \tag{2}$$

where Q_0 is a normalization constant, α is the absorption coefficient, and ω_0 is the laser beam spot size. The normalization constant can be calculated using the following relations [31]:

$$Q_0=P/2\pi G,\quad G=\int_0^a\exp\left(-2r^2/\omega_0^2\right)r\mathrm{d}r\int_0^l\exp(-\alpha z)\mathrm{d}z\,, \tag{3}$$

where P is the green light power, and a and l are the crystal radius and length, respectively. With a source term given in Eq. (2), the heat equation becomes a long transient equation [39]. The temperature dependence of thermal conductivity is given by [22, 36, 37]:

$$K(T) = \frac{K_0}{T_0 + \Delta T}, \tag{4}$$

where K_0 is the thermal conductivity at T_0=300 K, and ΔT is the temperature change. By considering a temperature-dependent thermal conductivity (described in Eq. (4)), Eq. (1) becomes:

$$\rho c \frac{\partial T}{\partial t} - \left(\vec{\nabla} K(T) . \vec{\nabla} T + K(T) \vec{\nabla}^2 T \right) = Q(\vec{r}), \tag{5}$$

which in cylindrical coordinates takes the following form:

$$\rho c \frac{\partial T}{\partial t} - \left(\left\{ \frac{\partial K(T)}{\partial r}\frac{\partial T}{\partial r} + \frac{\partial K(T)}{\partial \varphi}\frac{\partial T}{\partial \varphi} + \frac{\partial K(T)}{\partial z}\frac{\partial T}{\partial z} \right\} + K(T)\left\{ \nabla_r^2 T + \nabla_\varphi^2 T + \nabla_z^2 T \right\} \right) = Q(r) \cdot \tag{6}$$

Since the heat is transferred from the central region of the crystal to the boundaries by conduction, and then is transferred to the environment by convection and radiation, the most general boundary condition can be written as [38]:

$$-K(T)\hat{\mathbf{n}}.\nabla T|_{\text{boundary}} = h(T - T_\infty)_{\text{boundary}} + \sigma\varepsilon \left(T^4 - T_s^4\right)_{\text{boundary}}, \tag{7}$$

where $\hat{\mathbf{n}}$ is an outward unit vector perpendicular to the crystal surface, h is the heat convection coefficient, ε is surface emissivity (ε=0.9), σ=5.669×10^{-8} W m^{-2} K^{-4} is the Stefan–Boltzmann constant, and T_∞ and T_S are the temperature of cooling fluid and environment, respectively. Different values for heat convection coefficient have been reported, depending on cooling mechanism. A value of h=10 W m^{-2} K^{-1} is a common value, which is used for cooling with air in a laboratory [2]. Other values, such as h=6.5 W m^{-2} K^{-1}have also been reported and used for solid-state crystals cooled with air [39]. If the crystal is covered with an indium foil that is in contact with copper itself, the heat transfer coefficients will be h=15,000 W m^{-2} K^{-1} [40]. However, Wang et al. [41] reported two other values of h=50 W m^{-2} K^{-1} and h=20,000 W m^{-2} K^{-1} for cooling with air and water, respectively. Therefore, to cover all reported and practical values of heat convection coefficient, we will apply all of them in our calculations and their impact will be discussed. The presence of T^4 terms in the radiation boundary condition (Eq. (7)) makes it impossible to present an analytical solution for the temperature. Figure 1 shows the geometry and boundary conditions for the crystal used. The lateral surface of the crystal is kept to a constant temperature (T_0=300 K) via using a cooling fluid flowing around the crystal.

3 Numerical Procedure

Due to the azimuthal symmetry of the crystal and heating source, the φ part in the heat equation can be dropped. Figure 2 shows a cross-section (r–z plane) of the cylindrical crystal under consideration along with temperature boundary conditions. Hence, Eq. (6) is rearranged as:

$$\rho c \frac{\partial T}{\partial t} - \left\{ \left(\frac{\partial K(T)}{\partial r}\frac{\partial T}{\partial r} + \frac{\partial K(T)}{\partial z}\frac{\partial T}{\partial z} \right) + K(T)\left(\frac{1}{r}\frac{\partial T}{\partial r} + \frac{\partial^2 T}{\partial r^2} + \frac{\partial^2 T}{\partial z^2} \right) \right\} = Q(\vec{r}), \tag{8}$$

Using finite difference method, Eq. (8) can be discretized to the following expression:

$$\begin{aligned} T(i+1,j,k) = {} & T(i,j,k) \\ & + \frac{\Delta t}{\rho c}\frac{T(i,j+1,k) - T(i,j-1,k)}{2\Delta r}\frac{K(j+1,k) - K(j-1,k)}{2\Delta r} \\ & + \frac{\Delta t}{\rho c}\frac{T(i,j,k+1) - T(i,j,k-1)}{2\Delta z}\frac{K(j,k+1) - K(j,k-1)}{2\Delta z} \\ & + \frac{\Delta t K(T)}{\rho c}\left(\frac{T(i,j-1,k) - 2T(i,j,k) + T(i,j+1,k)}{\Delta r^2} \right. \\ & \left. + \frac{T(i,j+1,k) - T(i,j-1,k)}{2r_j \Delta r} \right. \\ & \left. + \frac{T(i,j,k-1) - 2T(i,j,k) + T(i,j,k+1)}{\Delta z^2} \right) \\ & + Q(j,k)\frac{\Delta t}{\rho c}, \end{aligned} \tag{9}$$

where Δt, Δr, and Δz are time, radial distance, and longitudinal distance steps, respectively. Furthermore, the boundary condition equation takes the following form:

$$\begin{aligned} & -K(T)(\mp \hat{z}).\left(\frac{\partial T}{\partial r}\hat{r} + \frac{\partial T}{\partial \varphi}\hat{\varphi} + \frac{\partial T}{\partial z}\hat{z} \right)\Big|_{\text{boundary}} \\ & \quad = \left[h(T - T_\infty) + \sigma\varepsilon\left(T^4 - T_s^4\right) \right]_{\text{boundary}}, \end{aligned} \tag{10}$$

Considering $\hat{z}.\,r = \hat{z}\,.\,\hat{\varphi} = 0$, we end up with:

$$\left.\frac{\partial T}{\partial z}\right|_{z=0} = \left.\frac{h(T - T_\infty) + \sigma\varepsilon\left(T^4 - T_s^4\right)}{K(T)}\right|_{z=0}, \tag{11}$$

and

$$\left.\frac{\partial T}{\partial z}\right|_{z=l} = -\left.\frac{h(T - T_\infty) + \sigma\varepsilon\left(T^4 - T_s^4\right)}{K(T)}\right|_{z=l}, \tag{12}$$

for entrance and end face of crystal, respectively. Since, in factual situations, the lateral surface of the crystal gets cold by

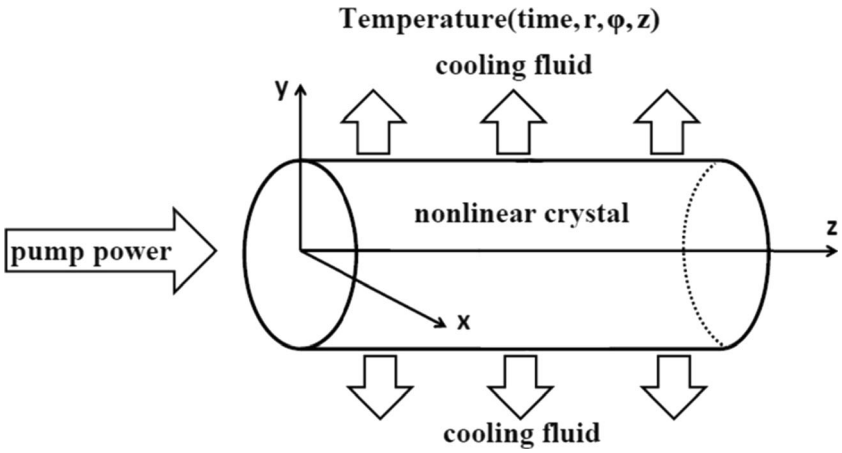

Fig. 1 The geometry and the puming scheme of the crystal. The cooling fluid flowing around the crystal keeps the lateral temperature constant

a coolant, the constant temperature boundary condition can be adopted at $r=a$. Therefore, we have:

$$T(r=a,z,t)=T_0=300\ \text{K} \tag{13}$$

The thermal and optical properties of KTP used in this work are listed in Table 1.

4 Results and Discussions

Finite difference method was used to solve the transient heat equation. A home-made code was written in Fortran (Ifort) and run in the Linux operating system. The crystal under simulation was a cylindrical KTP with a radius of a=2 mm and a length of l=20 mm [17]. To show the radiation effect on the crystal temperature, another radius of 5 mm was also taken for the crystal. A TEM_{00} Gaussian heat source was considered with a power of P=80 W and beam spot sizes of ω_f=100 mm and 3 mm [17]. The latter is used, again, to highlight the radiation effects. With the physical and geometrical specifications used, the crystal was divided in 200×150 ($r\times z$) meshes to reach a high accuracy. To insure about stability of the problem, time step was chosen to be $\Delta t=6.97\times10^{-6}$ s. Every run took 360 s with a computational machine with an Intel(R) Core (TM) i5 CPU 2.53 GH and 4 GB RAM. Of course, this is a time for an optimized code.

Figure 3 shows the variations of KTP thermal conductivity against the temperature. The figure clearly reveals a noticeable difference between a constant thermal conductivity and a temperature-dependent thermal conductivity.

Figure 4 shows the variations of the temperature of the crystal with radius of a=2 mm at z=0 and r=0 versus the time. In this figure, the beam spot size has been taken to be ω= 100 μm. To plot the curves, the radiation as well as the convection has been considered. As the Fig. 4 shows, since the crystal is in thermal equilibrium with the environment, prior to switching the heat source on, the crystal temperature starts from 300 K. It grows and reaches a constant value, which is dependent on the ambient temperature and thermal properties of the crystal. This is the steady-state value of temperature, that is, if one solves the steady-state heat equation, this result will be obtained. Moreover, Fig. 4 reveals a noticeable difference between considering a constant thermal conductivity and a temperature-dependent one. It is obvious that considering a temperature-dependent thermal conductivity leads to a ~ 69.22 K difference between two cases. Being cautious about KTP damage, this difference is significantly important.

Figure 5 shows the crystal temperature as a function of radial distance at the crystal entrance face [surface (B)] after reaching steady state. This figure shows that the temperature at the surface (B) is maximum, as a result of concentration of the heat energy at the center and not at the boundaries. As the radial distance is increased, the temperature drops down.

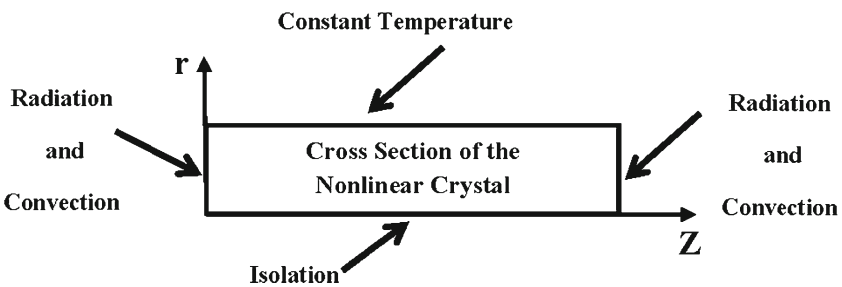

Fig. 2 The schematic illustration of the cylinder crystal. Due to azimuthal symmetry of crystal and pumping source, only r–z plane is used in the calculations. The temperature boundary conditions are specified at sides of simulation domain

Table 1 The thermal and optical properties of KTP

Quantity	Values	Reference
Thermal conductivity in 300 K	13 J kg^{-1} K^{-1}	[11]
Absorption coefficient at 532 nm	4 m^{-1}	[42, 43]
Specific heat	728.016 J m^{-1} K^{-1}	[11, 42]
Mass density	2945 kg/m^3	[11]

At $r=a$, the crystal temperature reaches 300 K (ambient temperature). The effect of temperature dependence of thermal conductivity is illustrated, which is more pronounced around the crystal center.

Figure 6 shows the steady-state crystal temperature on the z-axis (line C in Fig. 6) as a function of z, when the thermal conductivity is assumed to be constant (red dashed curve), and when the temperature dependence of thermal conductivity is considered (black solid curve). For temperature-dependent thermal conductivity case, the temperature is overall higher than that of temperature-independent case. For 80 W heating power, an overall 70 K difference in temperature is observed.

In Figs. 3, 4, 5, and 6, we used a value of $h=10$ W m^{-1} K^{-1} corresponding to cooling the crystal with air [2, 34]. To see the effect of other cooling mechanisms discussed in the previous section, we used also the heat convection coefficients of $h=6.5, 27.5, 50, 15{,}000$ and 20,000 W m^{-2} K^{-1} reported in literature [2, 39–41] to cover all practical situations. Figure 7 compares the temperatures corresponding to different values of h at the input facet of the crystal. As the figure shows, for $h=6.5, 10, 27.5$ and 50 W m^{-2} K^{-1}, the temperature distributions are the same and the difference can hardly be seen. But for $h=15{,}000$ and 20,000 W m^{-2} K^{-1}, different temperatures occur. Therefore, it is safe to say

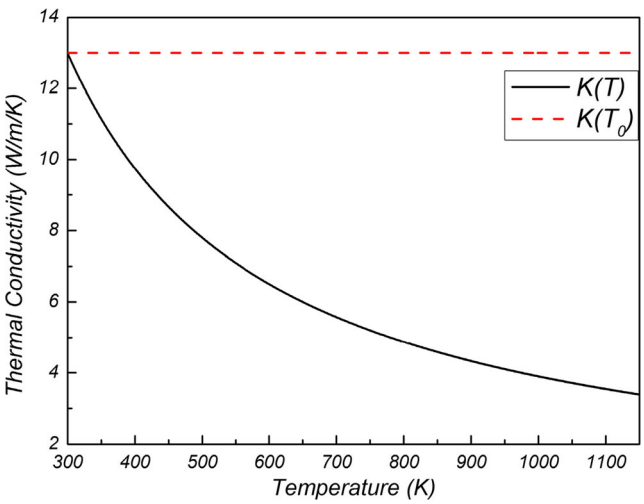

Fig. 3 Thermal conductivity of the KTP crystal as a constant (*broken lines*) and as a temperature-dependent variable (*black curve*)

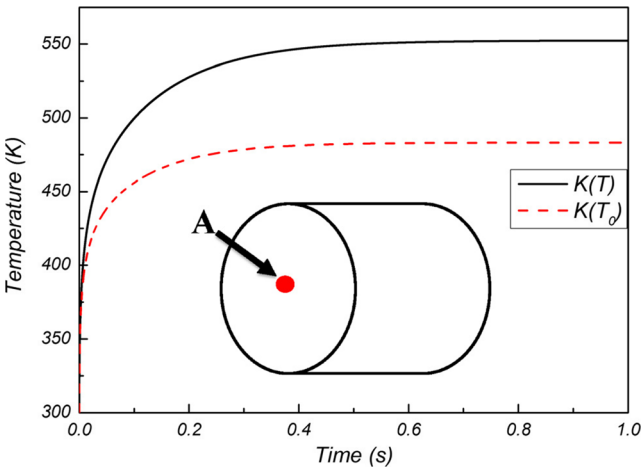

Fig. 4 The temporal temperature at the central point of entrance surface of the KTP crystal (*point A*) with constant thermal conductivity (*broken lines*) and temperature-dependent thermal conductivity (*black curve*)

that for the first set of the heat convection coefficients, a same temperature is obtained, that is, the problem is not sensitive to the h values in a 6.5 to 50 W m^{-2} K^{-1} interval. For $h=15{,}000$ and 20,000 W m^{-2} K^{-1}, approximately 20 K difference is seen. Overall, perfect cooling mechanism ($h=15{,}000$ and 20,000 W m^{-2} K^{-1}) can reduce the temperature by an amount of 20 K relative to cooling with air ($h=6.5, 10, 27.5$ and 50 W m^{-2} K^{-1}).

In all previous figures, the radiation as well as the convection boundary condition has been taken into account together. Hereafter, to show the role of the radiation on the temperature distribution, we use two sets of boundary conditions: convection with radiation and convection without radiation. These choices allow us to examine the role of radiation in the cooling of the crystal. The effect of heat radiation from the crystal surface on the temperature has been examined in Figs. 8, 9,

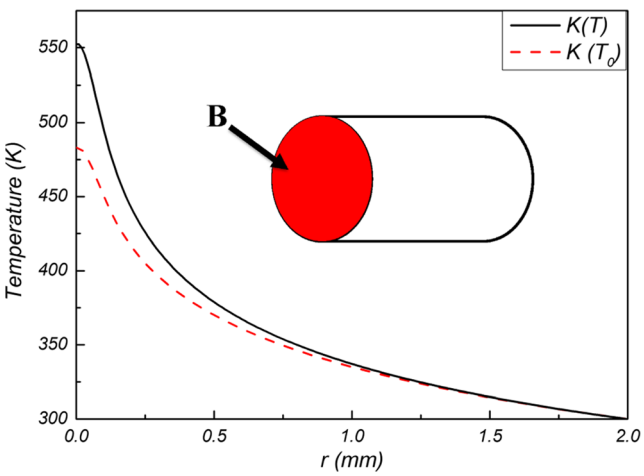

Fig. 5 The crystal temperature as a function of radial distance in entrance surface (surface B) for constant (*red curve*) and temperature-dependent (*black curve*) thermal conductivity

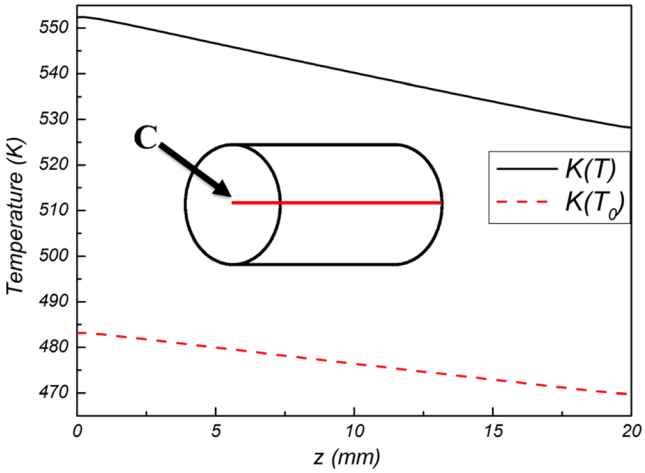

Fig. 6 The crystal temperature along the crystal length with constant thermal conductivity (*red curve*) and temperature-dependent thermal conductivity (*black curve*)

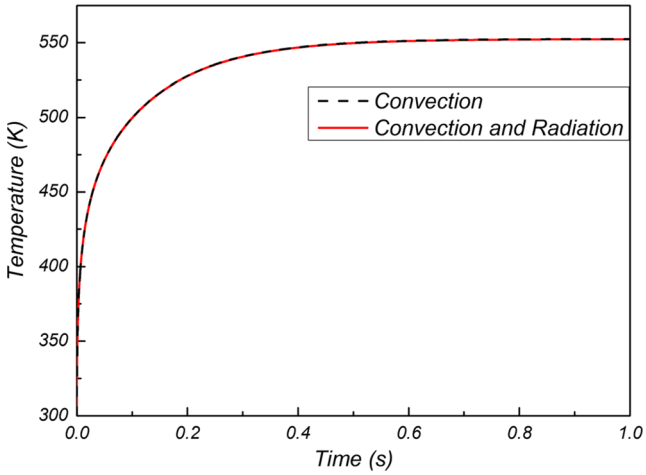

Fig. 8 The temporal temperature at the center of input surface of KTP crystal considering convection boundary condition (*black curve*) and both radiation- and convection-boundary conditions (*red curve*)

and 10 for a crystal with radius of a=2 mm and laser beam spot size of ω=100 μm, where the crystal temperature as a function of time (Fig. 8), radial distance (Fig. 9), and longitudinal distance (Fig. 10) are plotted. As these figures show, considering the radiation boundary conditions does not present any noticeable difference with the case in which it is discarded. Higher heat powers have also been examined to be sure about this statement shown in Figs. 11 and 12, that is, the temperature is plotted versus the time for two heat powers of 120 and 200 W at the point (A).

So far, the radiation has not shown any significant effect on the temperature distribution of a crystal with radius of a=2 mm and laser beam spot size of ω=100 μm, even with increasing the heating power. However, our calculations show that under certain conditions, the radiation can be influential. For a crystal with radius of a=5 mm irradiated with a laser beam with a spot size of ω=3 mm and heat power of 530 W, the radiation can show itself as a significant reduction in the temperature at the crystal beginning and end faces. Figure 13 shows the temperature along the crystal axis at r=0 for two cases of convection without radiation (black solid curve) and convection with radiation (red dashed curve). As the figure shows, the heat radiation from a larger surface considering a larger beam spot size results in a reduction of the temperature with a ~15 K at the input facet and a ~10 K at the output facet. The figure, however, indicates that for middle points of the crystal, the temperatures are the same, whether or not the radiation is taken into account.

Therefore, it can be concluded that considering the radiation boundary condition for crystals with small radii cannot be influential in the temperature distribution of the crystal. As a result, less numerical complexity will be encountered for this type of problem. However, for large radii along with large laser beam spot sizes, radiation can be effective on the

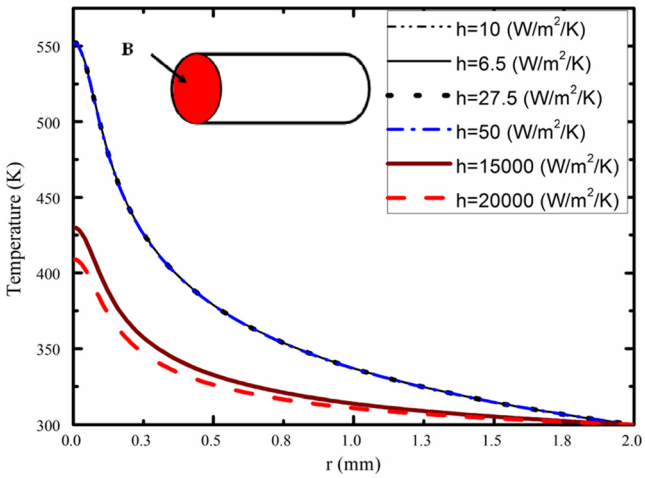

Fig. 7 The crystal temperature at the input facet of the crystal for different values of heat convection coefficient. The temperature-dependent thermal conductivity has also been used

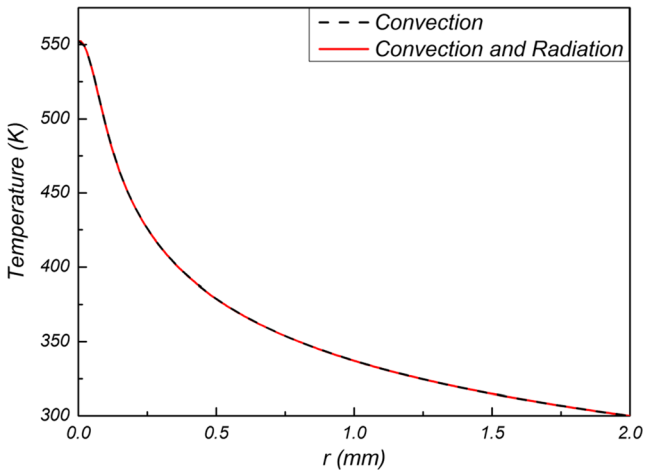

Fig. 9 The crystal temperature along the radial distance at the entrance surface considering convection boundary condition only (*black curve*) and both radiation- and convection-boundary conditions (*red curve*)

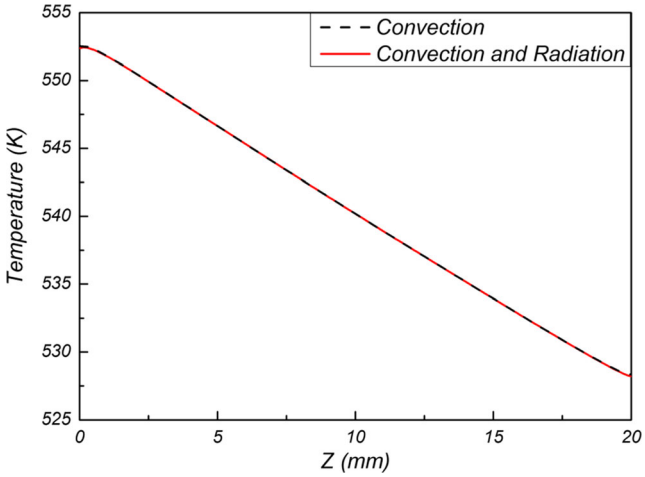

Fig. 10 The crystal temperature long the crystal length considering the convection boundary condition only (*black curve*) and both the radiation- and convection-boundary conditions (*red curve*)

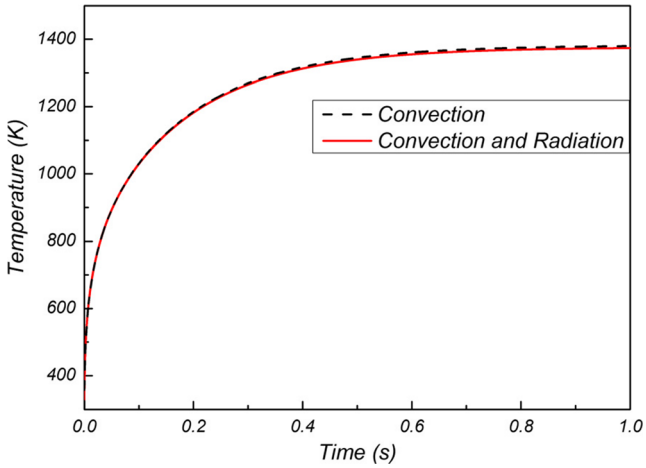

Fig. 12 The temporal temperature at the center of entrance surface of KTP crystal considering convection boundary condition only (*dashed black curve*) and both radiation- and convection-boundary conditions (*solid red curve*) for 200 W pump power

temperature distribution. We notice that the convection always plays its crucial role in determining the temperature, which has been discussed fully in [31, 39].

5 Conclusion

In this work, the transient heat equation for a KTP crystal under an end-pumped CW Gaussian thermal source was solved. The temperature dependence of thermal conductivity and heat radiation boundary condition were examined in detail in determining the crystal temperature. It was shown that considering the temperature-dependent nature of thermal conductivity leads to considerable differences with the case in which the thermal conductivity is considered to be constant. This situation is in sharp contrast to fiber lasers in which the variation of thermal conductivity with temperature emerging from the inherent properties of silica glass is not effective [34]. This conclusion is of great importance especially for developing accurate models. Moreover, it was shown that considering the radiation boundary condition for crystals with small radii and small laser beam spot sizes leads to no appreciable differences compared to a case in which it is ignored. This situation is, of course, again in sharp contrast to the fiber laser case in which radiation plays a crucial role in determining the temperature of the medium [33, 34]. In the case of crystals, it results from the small surface/volume ratio, which prevents huge radiation from the surface. However, increasing those surfaces of the crystal from which radiation occurs, radiation becomes important to achieve a realistic value for temperature. In fact, this case simulates the fiber case in which surface for radiation is large enough. The results of this work can help

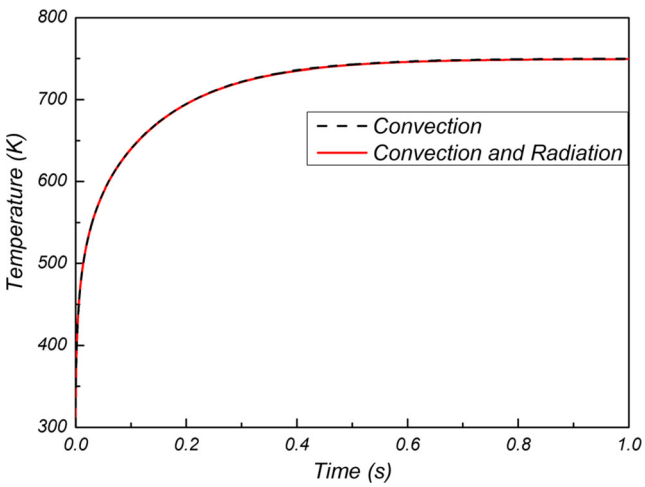

Fig. 11 The temporal temperature at the center of entrance surface of KTP crystal considering convection boundary condition only (*dashed black curve*) and both radiation- and convection-boundary conditions (*solid red curve*) for 120 W pump power

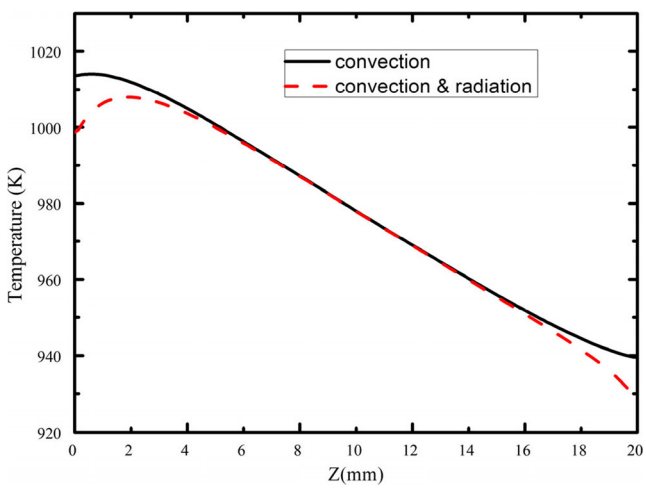

Fig. 13 The temperature distribution along the crystal axis with a radius of a=5 mm and a beam spot size of w=3 mm when convection only (*solid*) and convection with radiation (*dashed curve*) are considered

laser designers attempting to include thermal effects in their setups.

Acknowledgments Authors would like to thank Shahid Chamran University of Ahvaz, Iran, for supporting this work.

References

1. E. Garmire, Nonlinear optics in daily life. Opt. Express **21**, 30532–30544 (2013)
2. S. Kumar, S. Sabouri, A. Khorsandi, M. Ebrahim-Zadeh, Thermal effects in high-power continuous-wave single-pass second harmonic generation. IEEE J. Sel. Top. Quantom. Electron. pp. 563–572, (2014)
3. S.C. Kumar, G. Samanta, M. Ebrahim-Zadeh, High-power, single-frequency, continuous-wave second-harmonic-generation of ytterbium fiber laser in PPKTP and MgO: sPPLT. Opt. Express **17**, 13711–13726 (2009)
4. S.C. Kumar, G. Samanta, K. Devi, M. Ebrahim-Zadeh, High-efficiency, multicrystal, single-pass, continuous-wave second harmonic generation. Opt. Express **19**, 11152–11169 (2011)
5. M. Tsunekane, H. Inaba, N. Taguchi, High-power, efficient, low-noise, continuous-wave all-solid-state Ti: sapphire laser. Opt. Lett. **21**, 1912–1914 (1996)
6. X. Guo, W. Hou, H. Peng, H. Zhang, G. Wang, Y. Bi et al., 4.44 W of CW 515 nm green light generated by intracavity frequency doubling Yb: YAG thin disk laser with LBO. Opt. Commun. **267**, 451–454 (2006)
7. B. Lu, H. Chen, S. Wang, M. Jiang, Z. Ren, J. Bai, Red and green dual-wavelength laser based on LD side-pumped ceramic Nd: YAG and BBO electro-optical Q-switch. Opt. Laser Technol. **50**, 163–166 (2013)
8. H. Zhao, K. Sukhoy, I. Lima Jr., A. Major, Generation of green second harmonic with 60 % conversion efficiency from a Q-switched microchip laser in MgO: PPLN crystal. Laser Phys. Lett. **9**, 355 (2012)
9. J. Zheng, S. Zhao, Q. Wang, X. Zhang, L. Chen, Influence of thermal effect on KTP type-II phase-matching second-harmonic generation. Opt. Commun. **199**, 207–214 (2001)
10. D.-G. Xu, J.-Q. Yao, B.-G. Zhang, R. Zhou, E. Li, S.-Y. Zhao et al., 110 W high stability green laser using type II phase matching $KTiOPO_4$ (KTP) crystal with boundary temperature control. Opt. Commun. **245**, 341–347 (2005)
11. J.D. Bierlein, H. Vanherzeele, Potassium titanyl phosphate: properties and new applications. JOSA B **6**, 622–633 (1989)
12. D. Zhang, J. Lu, B. Feng, J. Zhang, Increased temperature bandwidth of second harmonic generator using two $KTiOPO_4$ crystals cut at different angles. Opt. Commun. **281**, 2918–2922 (2008)
13. P. Shi, W. Chen, L. Li, A. Gan, Semianalytical thermal analysis of thermal focal length on Nd: YAG rods. Appl. Opt. **46**, 6655–6661 (2007)
14. Z. Li, X. Huai, Y. Tao, Z. Guo, Analysis of thermal effects in an orthotropic laser medium. Appl. Opt. **48**, 598–608 (2009)
15. M. Sabaeian, F. Sedaghat Jalil-Abadi., M. Mohammad Rezaee, A. Motazedian, Heat coupled Gaussian continuous-wave double-pass type-II second harmonic generation: inclusion of thermally induced phase mismatching and thermal lensing. Opt. Express, **22**, 25615-25628 (2014).
16. M. Schmid, T. Graf, H. Weber, Analytical model of the temperature distribution and the thermally induced birefringence in laser rods with cylindrically symmetric heating. JOSA B **17**, 1398–1404 (2000)
17. M. Sabaeian, L. Mousave, H. Nadgaran, Investigation of thermally-induced phase mismatching in continuous-wave second harmonic generation: a theoretical model. Opt. Express **18**, 18732–18743 (2010)
18. Z. Cong, X. Zhang, Q. Wang, Z. Liu, X. Chen, S. Fan et al., Theoretical and experimental study on the Nd: YAG/$BaWO_4$/KTP yellow laser generating 8.3 W output power. Opt. Express **18**, 12111–12118 (2010)
19. R. Bhandari, T. Taira, 6 MW peak power at 532 nm by using linearly polarized passively Q-switched microchip laser. in *The European Conference on Lasers and Electro-Optics*, (2011), p. CA7_6
20. R. Weber, B. Neuenschwander, M. Mac Donald, M. Roos, H.P. Weber, Cooling schemes for longitudinally diode laser-pumped Nd: YAG rods. Quantum Electron. IEEE J. **34**, 1046–1053 (1998)
21. J.D. Beasley, Thermal conductivities of some novel nonlinear optical materials. Appl. Opt. **33**, 1000–1003 (1994)
22. C. Pfistner, R. Weber, H. Weber, S. Merazzi, R. Gruber, Thermal beam distortions in end-pumped Nd: YAG, Nd: GSGG, and Nd: YLF rods. Quantum Electron. IEEE J. **30**, 1605–1615 (1994)
23. S. Seidel, G. Mann, Numerical modeling of thermal effects in nonlinear crystals for high-average-power second harmonic generation. in *Photonics West'97*, (1997), pp. 204–214
24. R. Weber, B. Neuenschwander, H. Weber, Thermal effects in solid-state laser materials. Opt. Mater. **11**, 245–254 (1999)
25. M. Shimosegawa, T. Omatsu, M. Tateda, I. Ogura, J.L. Blows, P. Wang et al., Thermal conductivity of a self-frequency-doubling laser crystal measured by use of optical methods. Appl. Opt. **40**, 1372–1377 (2001)
26. B.A. Usievich, V.A. Sychugov, F. Pigeon, A. Tishchenko, Analytical treatment of the thermal problem in axially pumped solid-state lasers. IEEE J. Quantum Electron. **37**, 1210–1214 (2001)
27. Z. Xiong, Z.G. Li, N. Moore, W. Huang, G. Lim, Detailed investigation of thermal effects in longitudinally diode-pumped Nd: YVO 4 lasers. Quantum Electron. IEEE J. **39**, 979–986 (2003)
28. D. Xu, J. Yao, B. Zhang, S. Zhao, R. Zhou, X. Ding et al., Influence of the KTP crystal boundary temperature on conversion efficiency in high power green laser. Chin. Opt. Lett. **3**, 85–88 (2005)
29. T. Li, Z. Zhuo, X. Li, H. Yang, Y. Zhang, Study on optical characteristics of Nd: YVO_4/YVO_4 composite crystal laser. Chin. Opt. Lett. **5**, 175–177 (2007)
30. P. Shi, W. Chen, L. Li, A. Gan, Semianalytical thermal analysis on a Nd: YVO_4 crystal. Appl. Opt. **46**, 4046–4051 (2007)
31. M. Sabaeian, H. Nadgaran, L. Mousave, Analytical solution of the heat equation in a longitudinally pumped cubic solid-state laser. Appl. Opt. **47**, 2317–2325 (2008)
32. A. Sayahian Jahromi, M. Sabaeian, H. Nadgaran, Heat coupled laser rate equations: a model for Er-doped fiber lasers. Opt. Commun. **311**, 134–139 (2013)
33. M. Sabaeian, The effects of air-holes on temperature and temperature gradient of solid-core photonic crystal fiber lasers. Optik-Int. J. Light Electron. Opt. **124**, 5787–5791 (2013)
34. L. Mousavi, M. Sabaeian, H. Nadgaran, Thermally-induced birefringence in solid-core photonic crystal fiber lasers. Opt. Commun. **300**, 69–76 (2013)
35. M. Sabaeian, H. Nadgaran, An analytical model for finite radius dual-beam mode-mismatched thermal lens spectroscopy. J. Appl. Phys. **114**, 133102 (2013)
36. H. Glur, R. Lavi, T. Graf, Reduction of thermally induced lenses in Nd: YAG with low temperatures. IEEE J. Quantum Electron. **40**, 499–504 (2004)
37. C. Ong, E. Sin, H. Tan, Heat-flow calculation of pulsed excimer ultraviolet laser's melting of amorphous and crystalline silicon surfaces. JOSA B **3**, 812–814 (1986)
38. D.C. Brown, H.J. Hoffman, Thermal, stress, and thermo-optic effects in high average power double-clad silica fiber lasers. IEEE J. Quantum Electron. **37**, 207–217 (2001)
39. M. Sabaeian, Analytical solutions for anisotropic time-dependent heat equations with Robin boundary condition for cubic-shaped solid-state laser crystals. Appl. Opt. **51**, 7150–7159 (2012)

40. X. Peng, A. Asundi, Y. Chen, Z. Xiong, Study of the mechanical properties of Nd: YVO_4 crystal by use of laser interferometry and finite-element analysis. Appl. Opt. **40**, 1396–1403 (2001)
41. Y.-Y. Wang, D.-G. Xu, C.-M. Liu, W.-P. Wang, J.-Q. Yao, A high-power high-stability Q-switched green laser with intracavity frequency doubling using a diode-pumped composite ceramic Nd: YAG laser. Chin. Phys. B **21**, 4212 (2012)
42. D. N. Nikogosyan, *Nonlinear Optical Crystals: A Complete Survey: A Complete Survey* (Springer, Berlin, 2006)
43. P. Perkins, T. Fahlen, 20-W average-power KTP intracavity-doubled Nd: YAG laser. JOSA B **4**, 1066–1071 (1987)